# Optimization of the heat transfer simulation time during 3D printing of PLA material

Kandy Benié[1,2], Abel Cherouat[1], Thierry Barrière[2] and Vincent Placet[2]

[1] Université de Technologie de Troyes, Laboratory of Automatic Generation of Meshing and Advanced Methods (UR-GAMMA3), 12 rue Marie Curie, 10300 Troyes, France
[2] Université Bourgogne Franche-Comté, FEMTO-ST Institute, CNRS/UFC/ENSMM/UTBM, Department of Applied Mechanics (DMA), 24 chemin de l'épitaphe, 25000 Besançon, France
kandy.benie@utt.fr

**Abstract.** This work focused on optimizing the simulation time for heat transfer during the Fused Deposition Modeling process, which is necessary for a recent tensile property optimization study mentioned in the literature. The approach for optimizing the simulation time involved conducting a comparative analysis of various mesh sizes and simulation step times, assessing their influence on the resulting temperature profiles. The heat transfer simulation of the printed material was done with COMSOL Multiphysics FEA and the normal and extremely fine meshes as well as the simulation step times of $\Delta t$ =0.01 s and 0.05 s were considered. The results showed that all the combinations resulting from these simulation parameters were equivalent in terms of both temperature profile results and the results of the tensile property optimization study, but that the simulation time was minimized by using the normal mesh with $\Delta t$ = 0.05 s with a simulation time ten times shorter than in the case of the extremely fine mesh with $\Delta t$ = 0.01 s.

**Keywords:** 3D Printing, Heat Transfer, Simulation Time.

## 1 Introduction

Manufacturing a part can be done subtractively, formatively or additively. Additive manufacturing, more commonly known as 3D printing in a non-technical context, is the most recent of these methods and is increasingly used in major industries. Fused Deposition Modeling (FDM) is the most widely used additive manufacturing process for rapid prototyping. It involves passing solid polymer material through a heated cavity where the material is melted and extruded through a nozzle. The extruded material is then deposited on the printing plate according to the desired geometry to build the final 3D part layer by layer [1]. This operating principle means that the part produced by 3D printing is composed of several layers that are made up of partially bonded strands (Fig. 1). This partial bonding between the strands makes the mechanical properties of the 3D parts depend on the mechanical properties of the printed material, the void between the strands and the strand-to-strand bond strength [2].

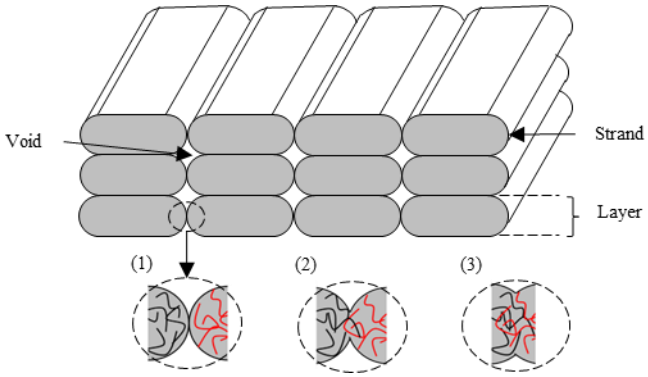


**Fig. 1.** Bond formation process through sintering: (1) Surface contact; (2) Bond formation and molecular diffusion at the interface; (3) Bond and molecular diffusion growth.

This makes the mechanical properties of parts made by 3D printing inferior to those of conventional processes such as injection and thermoforming process for plastic parts [3]. However, many authors have shown that the printing parameters used affect the mechanical properties of the printed parts [4]. However, due to the interdependence of these parameters, it is difficult to precisely identify their influence on the mechanical properties, and thus to choose the optimal printing parameters. To overcome this problem, Benié et al. [5] have proposed a study to identify the printing parameters allowing to maximize the mechanical properties of the printed parts without having to carry out costly and time-consuming experiments.

The aim of this work was to define an optimization parameter linked to the printing parameters, the value of which would be an indicator of the mechanical performance of the printed part. To achieve this, the main physical phenomena involved in printing, namely diffusion, coalescence and crystallization, were studied. Contrary to the existing literature, where these phenomena were studied independently of one another (e.g. study of diffusion by [6], study of coalescence by [2], study of crystallization by [7]), the study proposed by Benié et al. consisted in coupling all these phenomena in order to derive a numerical value named DCC (Diffusion, Coalescence and Crystallization), whose maximization would lead to the best tensile properties. At the end of the study, it has been shown that the DCC values were excellent indicators of the mechanical performance of printed parts. However, a problem arises when determining this DCC parameter.

Indeed, the physical phenomena under consideration are temperature-dependent. Thus, to study them, as Fig. 2 shows, it is essential to know the temperature profile during 3D printing. Since the temperature profile was determined by numerical simulation, to identify the optimum DCC values, it is necessary to simulate the heat transfer for all the combinations studied. In [5] for example, sixteen-parameter combinations were studied with simulation times between 2 and 8 hours per combination, which is considerably high and makes the DCC study lose its time saving dimension.

In this paper, different mesh sizes and different simulation step times were studied in order to optimize the simulation time and to make the DCC study more interesting.

Although the approach proposed for this paper was basic, it achieved the desired objectives.

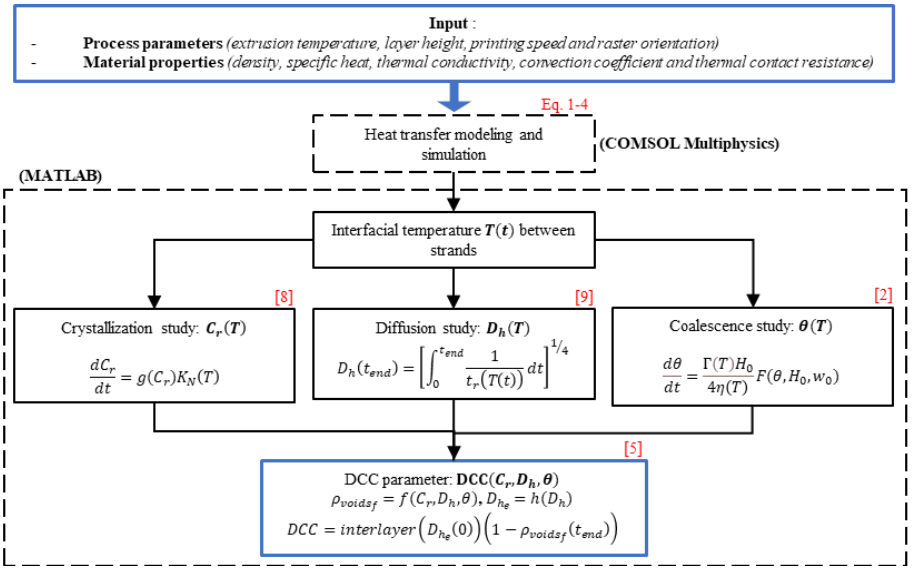


**Fig. 2.** Procedure for calculating the DCC parameter.

## 2 Modeling and numerical simulation

### 2.1 Modeling

In this paper, the model used was the same as that used by Benié et al. [5]. It is a 2D model based on the successive activation of the strands for each layer of printing part. Indeed, starting from a 2D geometry of the part to be printed, the strands of the part are activated one after the other in order to allow the heat exchange between the adjacent strands. To do this, the time required to go from one strand to another is determined before the numerical simulation.

During 3D printing, many authors have shown that the deposition of new strands tends to change the temperature in the previously printed strands. However, for the printing of intra-layer strands, this temperature modification can be neglected contrary to the case of inter-layer strands where the influence of the deposition of new strands is more pronounced. Indeed, the contact surface between the interlayer strands is very large compared to that of the intralayer strands. This leads to a higher heat exchange for the interlayer strands than for the intralayer strands. The work of Sun et al. [10] illustrates this well, since the temperature profile obtained experimentally when printing a 38 x 38mm x 30-layer part shows that the printing of interlayer strands leads to temperature peaks, whereas the printing of intralayer strands shows no peaks and was

not easily identifiable on the temperature profile. From this point of view, only two intralayer cords and all layers have been considered in the model as shown Fig. 3a.

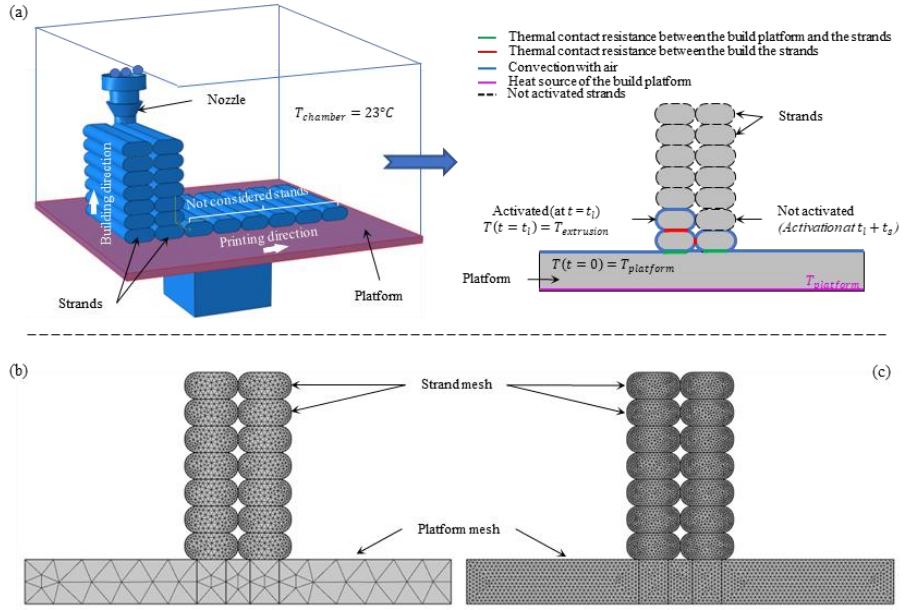


**Fig. 3.** (a) Initial and boundary conditions of the heat transfer during printing; (b) normal mesh (M1) and (c) extremely fine mesh (M2).

**Partial differential heat equation**: the heat conduction equation in the polymer domain was described by the partial differential equation of the transient conduction Eq. 1 where $\rho$ is the density, $C_p$ the specific heat and $k$ the thermal conductivity (the heat source term for the crystallization is supposed negligible).

$$\rho C_p(\dot{T}) = \vec{\nabla}.(k\vec{\nabla}T) \quad (1)$$

**The boundary and initial conditions** (Fig. 3a):

- The exposure of the external surface of the polymer to the air leads to its cooling by convection (the radiative effects are neglected) which is described by Eq. 2 as:

$$-k\vec{\nabla}T.\vec{n} = h(T - T_{chamber}) \quad (2)$$

  where $\vec{n}$ is the outward normal vector of domain and $h$ the convection heat transfer coefficient and $T_{chamber}$ is the temperature inside the chamber.
- The heat conduction between each domain in contact (strand-strand and build platform-stand) was given by Eq. 3 using the thermal contact resistances ($TCR$):

$$\begin{cases} -k_{strand}\vec{\nabla}T.\vec{n}_{strand} = \frac{1}{TCR_{strand}}(T^+ - T^-) & Strand - Strand \\ -k_{platform}\vec{\nabla}T.\vec{n}_{platform} = \frac{1}{TCR_{platform}}(T^+ - T^-) & Platform - Strand \end{cases} \quad (3)$$

where $T^+$ and $T^-$ are the temperatures on both sides of the interface. Low values of $TCR$ were considered and $TCR_{strand} = TCR_{platform}$ since their influences were negligible on the simulation results

- At initial time, the temperature in each domain was supposed to be known and uniform as (Eq. 4):

$$\begin{cases} T(t=0) = T_{extrusion} & On\ the\ new\ strand \\ T(t=0) = T_{platform} & On\ the\ build\ platform \end{cases} \quad (4)$$

Furthermore, it was assumed that the heat transfer was performed exclusively by thermal contact and convection, that the crystallization had no influence on the heat transfer and that the thermal properties of PLA were fixed during the heat transfer (Table 1).

**Table 1**. Thermal properties of material.

| Material | $\rho$ (kg/m$^3$) | $C_p$ (J/kg.K) | $k$ (W/m.K) | $h$ (W/m$^2$.K) | $TCR$ (m$^2$.K/W) |
|---|---|---|---|---|---|
| Strands: PLA | 1250 [11] | 1179 [11] | 0.28 [11] | 5 [12] | $10^{-5}$ [13] |
| Plate: PEI | 1270 [14] | 2000 [15] | 0.2 [15] | 5 [12] | $10^{-5}$ [13] |

## 2.2 Numerical simulation of 3D printing

To develop the finite element equations, the partial differential equations Eq. 1 must be restated in an integral form called the weak form. A weak form of the differential equations is equivalent to the governing equation and boundary conditions, i.e. the strong form. To solve the partial differential by the finite element method, we used the weighted residue method in the Galerkin formulation in which, we multiplied by an arbitrary temperature $T^*$ and integrate over the polymer domain S as Eq. 5:

$$W(T,T^*) = \iint_S T^* \left(\rho C_p(\dot{T}) - \vec{\nabla}.\left(k\vec{\nabla}T\right)\right) dS \qquad \forall\, T^* \quad (5)$$

The 2D numerical simulations were performed with COMSOL Multiphysics 6.0 using a time dependent study of the heat transfer in solids interface. The boundary conditions were implemented from the COMSOL integrated nodes of convection and thermal contact and the resolution method used was the implicit Backward Differentiation Formula (BDF) method.

The implicit method is to write the time derivative of the temperature as Eq. 6 where $\Delta t$ is the step time. Starting from the initial condition T(t=0), the nodal temperature is estimated at each instant by increments successive time Δt. This problem could be solved with direct integration methods over time (Euler method explicit or implicit, semi-explicit methods, the Crank–Nicholson method, etc.).

$$\dot{T} = \frac{T_{t+\Delta t} - T_t}{\Delta t} \quad (6)$$

Two predefined meshes in COMSOL were studied: the normal mesh M1 (212 triangular linear finite elements for each strand and the global model has 6925 dof) and the extremely fine mesh M2 (556 triangular linear finite elements for each strand and the global model had 41155 dof) as shown in Fig. **3**b-c. Also, two different simulation step times were studied: $\Delta t$ = 0.01 s and $\Delta t$ = 0.05 s.

For each of these cases, four combinations of printing parameters were considered. They are presented in Table 2. At the end of simulations, the temperatures at the interface of the strands were used from probes positioned at each thermal contact and measuring the average temperature of the interface to calculate the DCC parameter. Thus, the DCC values obtained were used to identify any correlation between the different simulation parameters. The simulations were performed on an Intel(R) Core(TM) i5-4590 CPU.

**Table 2**. Specimen nomenclature and printing parameters used for the study.

| Specimen | Raster orientation (°) (see Fig. ) | Extrusion Temperature (°C) | Printing speed (mm/s) | Layer height (mm) | Platform temperature (°C) |
|---|---|---|---|---|---|
| $A_L$ | 0 | 200 | 50 | 0.4 | 40 |
| $B_L$ | 0 | 200 | 50 | 0.6 | 40 |
| $A_T$ | 90 | 200 | 50 | 0.4 | 40 |
| $B_T$ | 90 | 200 | 50 | 0.6 | 40 |

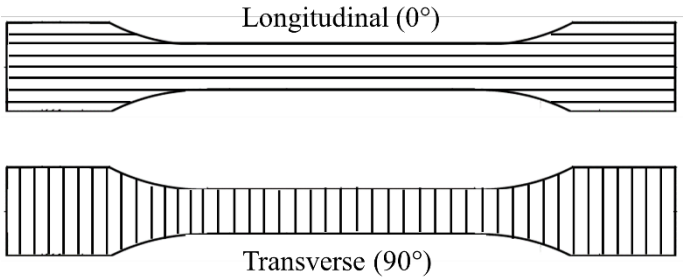


**Fig. 4.** Orientation of the strands in the specimens according to the raster orientation.

## 3 Results and discussions

To be able to validate the heat transfer simulation, a numerical simulation is conducted for a multi-layer wall manufactured by the FDM process. Note that the simulation is applied on ABS as material to be able to match the condition of existing experimental results in the literature. Fig. 5 represents the comparison of the results of numerical simulation and the results of an experimental study derived from the literature [13]. The agreement between the simulation and experimental results validates the heat transfer modeling approach conducted in this work.

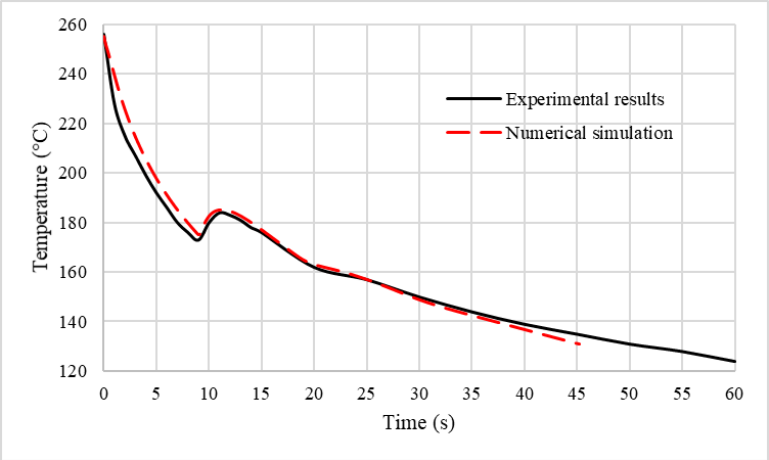


**Fig. 5.** Validation of the heat transfer model with experimental results derived from literature on a multi-layer wall geometry [13].

First of all, no convergence problems were encountered during the simulations. The results of the numerical simulation of the heat transfer presented in paragraph 2.b are shown in Table 3 for the specimen $B_T$ and showed that in a given strand the temperature was not uniform and that no heat transfer took place with non-activated strands until their activation.

**Table 3.** Iso-values of temperature during the printing of $B_T$ specimen with M1 mesh and $\Delta t$ = 0.05 s.

| t = 0.2 s<br>Layer 1/strand 1 printing | t = 0.25 s<br>Layer 1/strand 2 printing | t = 186 s<br>Layer 5/strand 2 printing |
|---|---|---|
| 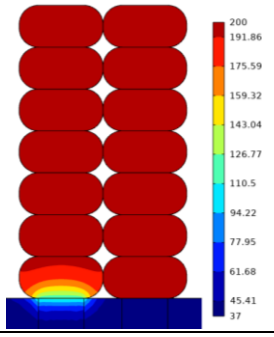 | 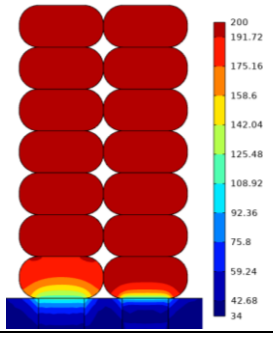 | 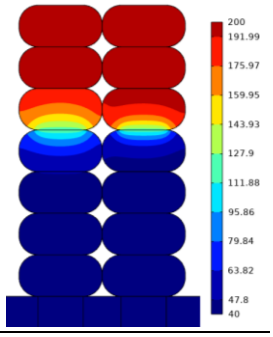 |
| t = 279 s<br>Layer 7/strand 2 printing | t = 280 s<br>Temperature during cooling | t = 325 s<br>Final temperature |

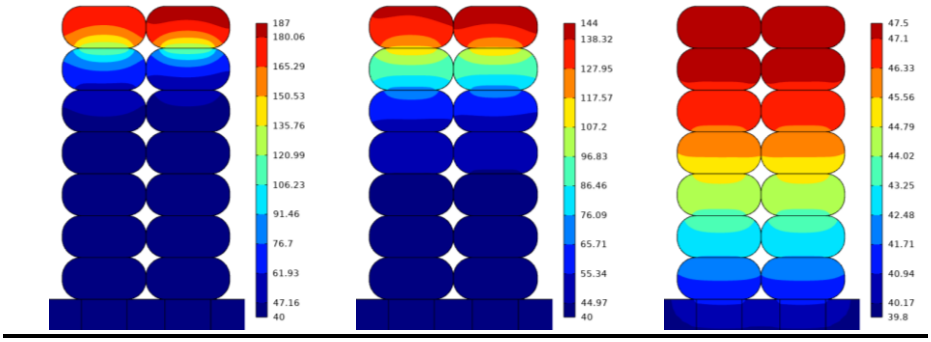


The temperature iso-values are given in Table 4 for the $B_T$ combination and show that regardless of the simulation parameters used, the final temperatures are almost identical. As well, to be more precise, the final values of the interfacial temperatures between the first two strands were collected for all combinations of printing parameters in order to identify the impact of the simulation parameters on the temperature. The results are presented in Table 5 and show that only the mesh size has an impact on the temperature although it is minimal. Indeed, for the same mesh size, the final interfacial temperature hardly varied when using a simulation step time $\Delta t$ of 0.01 s or 0.05 s. On the other hand, for a fixed simulation step time, moving from one mesh size to another led to a slight variation of the temperature of the order of 0.1°C maximum. This is negligible. Therefore, the interfacial temperature was only slightly affected by the simulation parameters used.

**Table 4.** Iso-value of temperature at the end of the simulation for $B_T$ specimen.

| | $\Delta t$ = 0.01 s | $\Delta t$ = 0.05 s |
|---|---|---|
| M1 mesh | 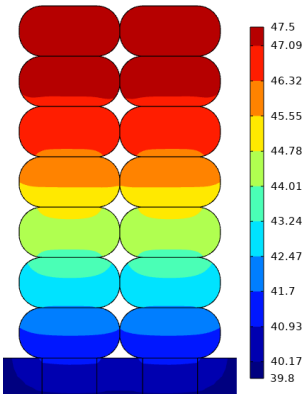 | 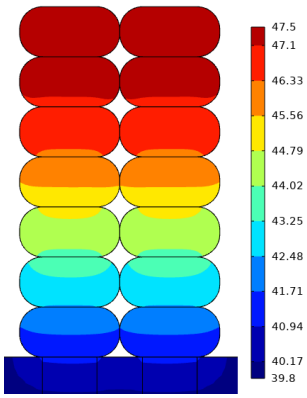 |

M2 mesh

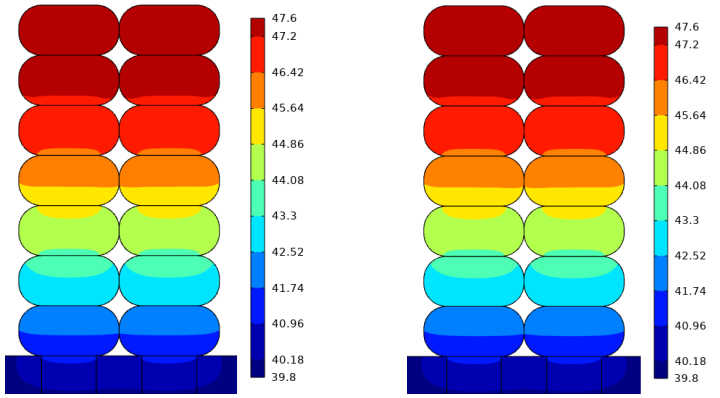


**Table 5.** Final interfacial temperatures for different simulation parameters.

| | M1 mesh | | M2 mesh | |
|---|---|---|---|---|
| Specimen | $\Delta t = 0.01$ s | $\Delta t = 0.05$ s | $\Delta t = 0.01$ s | $\Delta t = 0.05$ s |
| $A_L$ | 43.26°C | 43.26°C | 43.3°C | 43.3°C |
| $B_L$ | 47.88°C | 47.88°C | 47.98°C | 47.99°C |
| $A_T$ | 42.41°C | 42.41°C | 42.45°C | 42.45°C |
| $B_T$ | 46.55°C | 46.55°C | 46.64°C | 46.64°C |

For the different mesh sizes and simulation step times studied, the DCC parameter was determined for four combinations of printing parameters. The resulting DCC values were used to compare the simulation methods.

The results presented in Table 6 show that there was an excellent correlation between the DCC values obtained for different mesh sizes. Thus, using the extremely fine mesh or the normal mesh led to the same conclusions regarding the mechanical performance of the printed parts. Indeed, in both cases, the $A_L$ combination was the best (highest DCC value) and the $B_T$ combination was the worst (lowest DCC value).

Moreover, the correlation between the DCC values obtained in all cases was at least 0.9998 with respect to the most accurate case (extremely fine mesh and $\Delta t = 0.01$ s). This showed that all the simulation parameters studied here could be used for the DCC study and the interpretations of the final DCC results would be the same. In this sense, it is preferable to use simulation parameters that minimize the simulation time.

The lowest simulation time was obtained with the normal mesh and $\Delta t = 0.05$ s where the simulation lasted 26 min and 12 s for $A_L$ combination against 5 h 4 min and 5 s in the case of the longest simulation time with extremely fine mesh and $\Delta t = 0.01$ s. This means that the simulation time was divided by 11 between these two cases. The same was true for all combinations of printing parameters where there was a factor of at least 10 between the simulation times of these two cases without impacting the interpretation of the DCC values.

**Table 6.** Simulation times and DCC results obtained for different simulation parameters.

| | M1 mesh | | M2 mesh | |
|---|---|---|---|---|
| | $\Delta t = 0.01$ s | $\Delta t = 0.05$ s | $\Delta t = 0.01$ s | $\Delta t = 0.05$ s |
| Specimen | Simulation time | | | |
| $A_L$ | 2h42min26s | 26min12s | 5h04min05s | 1h46min03s |
| $B_L$ | 1h06min56s | 13min08s | 2h16min40s | 25min36s |
| $A_T$ | 3h25min55s | 26min48s | 5h15min18s | 52min51s |
| $B_T$ | 1h29min48s | 15min16s | 2h38min24s | 27min07s |
| | DCC values | | | |
| $A_L$ | 0.9472 | 0.9486 | 0.9478 | 0.9490 |
| $B_L$ | 0.9301 | 0.9318 | 0.9310 | 0.9324 |
| $A_T$ | 0.9168 | 0.9179 | 0.9170 | 0.9181 |
| $B_T$ | 0.9071 | 0.9083 | 0.9074 | 0.9085 |
| | | | $r^2$ | |
| | 0.9998 | 0.9999 | 1 | 0.9999 |

Tensile tests were carried out to determine the Young's moduli, maximum stresses and fracture strains of the different printing parameter combinations considered in this work. These tensile properties were then used to study their correlation with the DCC values. Thus, considering Table 7 presenting the values of the tensile properties for the four combinations of printing parameters and the correlation between these properties and the DCC values obtained for different simulation parameters, it appears that the correlations remained almost equivalent whatever the simulation parameters used for each tensile property. This means that for all simulation parameters the DCC values remained excellent indicators of mechanical performance.

Therefore, among the simulation parameters studied in this work, the normal mesh with $\Delta t = 0.05$ s is the best combination to optimize the simulation time in order to guarantee the time saving dimension of the DCC parameter besides being a good indicator of mechanical performances.

**Table 7.** Tensile properties of specimens and correlation between these properties and the DCC values obtained from different simulation parameters.

| | Specimen | Young's modulus (GPa) | Tensile strength (MPa) | Fracture strain (%) |
|---|---|---|---|---|
| | $A_L$ | $3.19 \pm 0.10$ | $45.1 \pm 1.8$ | $1.57 \pm 0.05$ |
| | $B_L$ | $3.11 \pm 0.08$ | $31.5 \pm 3.4$ | $1.03 \pm 0.13$ |
| | $A_T$ | $3.01 \pm 0.03$ | $25.5 \pm 0.9$ | $0.92 \pm 0.05$ |
| | $B_T$ | $2.94 \pm 0.11$ | $22.8 \pm 0.3$ | $0.83 \pm 0.04$ |
| | | $r^2$ with DCC values | | |
| M1 mesh | $\Delta t = 0.01$ s | 0.9958 | 0.9583 | 0.9001 |
| | $\Delta t = 0.05$ s | 0.9931 | 0.9552 | 0.8943 |
| M2 mesh | $\Delta t = 0.01$ s | 0.9933 | 0.9549 | 0.8937 |
| | $\Delta t = 0.05$ s | 0.9941 | 0.9526 | 0.8898 |

## 4 Conclusion

In this work, a study on the optimization of the simulation time of heat transfer during 3D printing has been carried out in order to guarantee the time saving in the identification of the printing parameters maximizing the mechanical properties of the printed parts through the DCC study introduced in [5].

To perform this study, a 2D model based on stepwise strand activation was used and the numerical simulation was performed under COMSOL Multiphysics 6.0 as in [5]. The optimization study was subsequently performed by varying the mesh size and simulation step time between two levels each: the mesh size between the normal and the extremely fine mesh integrated in COMSOL and the step time $\Delta t$ between 0.01 s and 0.05 s. For each of these simulation parameters, the temperature profiles from the numerical simulations for four combinations of printing parameters were used to determine the DCC values. From these DCC values obtained for all simulation parameters, correlation studies were performed to identify the influence of the simulation parameters on the DCC study.

During the simulations, no convergence problems were encountered and the results showed that for each combination of printing parameters studied, the final temperature values varied very little from one combination of simulation parameters to another. Also, it was shown that not only was there a very good correlation between the DCC values obtained from all the simulation parameter combinations with a coefficient of determination $r^2$ of at least 0.9998, but also that in all the simulation cases, the DCC parameter remained a good indicator of the mechanical performance of the printed parts. Therefore, any combination of simulation parameters studied could be used to perform the DCC study.

The major differentiation between the different simulation cases being the simulation time and in order to minimize it, in this work, the use of the normal mesh with $\Delta t = 0.05$ s was the best combination since the simulation time of this combination was the smallest and was at least ten times shorter than the longest simulation time for the combination using the extremely fine mesh with $\Delta t = 0.01$ s.

Thus, although the approach proposed in this article was basic, it was possible to give the DCC parameter its full value, which is to quickly determine the printing parameters that maximize the mechanical properties of the printed parts without performing material-intensive experiments.

## References

1. Brenken, B., Barocio, E., Favaloro, A., Kunc, V., Pipes, R., N.: Fused filament fabrication of fiber-reinforced polymers: a review. Addit. Manuf. 21, 1-16 (2018).
2. Garzon-Hernandez, S., Garcia-Gonzalez, D., Jérusalem, A., Arias, A.: Design of FDM 3D printed polymers: an experimental-modelling methodology for the prediction of mechanical properties. Mater. Des. 188, 108414 (2020).
3. Le Duigou, A., Correa, D., Ueda, M., Matsuzaki, R., Castro, M.: A review of 3D and 4D printing of natural fibre biocomposites. Materials and Design 194, 108911 (2020).

4. Dey, A., Yodo, N.: A systematic survey of FDM process parameter optimization and their influence on part characteristics. J. Manuf. Mater. Process. 3, 64 (2019).
5. Benié, K., Barrière, T., Placet, V., Cherouat, A.: Introducing a new optimization parameter based on diffusion, coalescence and crystallization to maximize the tensile properties of additive manufacturing parts. Addit. Manuf. 69, 103538 (2023).
6. Costa, S.,F., Duarte, J., F., Covas, J., A.: Estimation of filament and adhesion development in fused deposition techniques. J. Mater. Process. Technol. 245, 167–179 (2017).
7. Balani, S., B.: Additive manufacturing of the high-performance thermoplastics: experimental study and numerical simulation of the fused filament fabrication, Ph.D. Thesis. (2019).
8. Patel, R., M., Spruiell, J., E.: Crystallization kinetics during polymer processing – analysis of available approaches for process modeling. Polym. Eng. Sci. 31, 730–738 (1991).
9. Yang, F., Pitchumani, R.: Healing of thermoplastic polymers at an interface under nonisothermal conditions. Macromolecules 35, 3123–3224 (2002).
10. Sun, Q., Rizvi, G., M., Bellehumeur, C., T., Gu, P.: Effect of processing conditions on the bonding quality of FDM polymer filaments. Rapid Prototyp. J. 14, 72–80 (2008).
11. Noel, H., Sadou, A., Glouannec, P., Feller, J.,-B., Antar, Z.: Étude expérimentale des propriétés thermo-optiques de matériaux polymères composites pour la réalisation d'absorbeurs solaires. In Congrès Français de Thermique, SFT 2009, Vannes, 26-29 mai 2009.
12. Aressy, M.: Etude et modélisation de la cristallisation du Polylactide (PLA) en vue de l'optimisation du procédé de rotomoulage, Ph.D. Thesis. (2013).
13. Lepoivre, A., Boyard, N., Levy, A., Sobotka, V.: Heat transfer and adhesion study for the FFF additive manufacturing process. Procedia Manuf. 47, 948–955 (2020).
14. Li, M., Jiang, Z., Hu, B., Zhai, W.: Fused deposition modeling of hierarchical porous polyetherimide assisted by an in-situ CO2 foaming technology. Compos. Sci. Technol. 200, 108454 (2020).
15. PEI online supplier: thermal properties of PEI, https://www.azom.com/article.aspx?ArticleID=1883, last accessed 2022/05/22.